0026-895X/02/6202-210–219$7.00
MOLECULAR PHARMACOLOGY
Copyright © 2002 The American Society for Pharmacology and Experimental Therapeutics
Mol Pharmacol 62:210–219, 2002

Vol. 62, No. 2
1676/997367
Printed in U.S.A.

The Ca^{2+} Channel Antagonists Mibefradil and Pimozide Inhibit Cell Growth via Different Cytotoxic Mechanisms

GABRIEL E. BERTOLESI, CHANJUAN SHI, LINDSY ELBAUM, CHRISTINE JOLLIMORE, GABRIELA ROZENBERG, STEVEN BARNES, and MELANIE E. M. KELLY

Laboratory of Retina and Optic Nerve Research, Departments of Ophthalmology (G.E.B., C.S., C.J., S.B., M.E.M.K.), Pharmacology (G.E.B., C.S., L.E., C.J., M.E.M.K.), and Physiology & Biophysics (G.E.B., G.R., S.B.), Dalhousie University, Halifax, Nova Scotia, Canada

Received February 15, 2002; accepted April 25, 2002

This article is available online at http://molpharm.aspetjournals.org

ABSTRACT

We show that mitogenic cells expressing T-type Ca^{2+} channels (T-channels) are more sensitive to the antiproliferative effects of the drugs pimozide and mibefradil than cells without significant T-channel expression. The growth of Y79 and WERI-Rb1 retinoblastoma cells, as well as MCF7 breast cancer epithelial cells, all of which express T-channel current and mRNA for T-channel subunits, is inhibited by pimozide and mibefradil with IC_{50} values between 0.6 and 1.5 μM. Proliferation of glioma C6 cells, which show little T-channel expression, is less sensitive to these drugs (IC_{50} = 8 and 5 μM for pimozide and mibefradil, respectively). Neither drug seems to alter cell cycle or the expression of cyclins. Although this strong correlation between T-channel expression and growth inhibition exists, the following results suggest that the drugs inhibit cell growth via different cytotoxic pathways: 1) pimozide and mibefradil have additive effects on T-channel current inhibition, whereas the antiproliferative activity of the drugs together is synergistic; 2) an increase in the number of apoptotic Y79 and MCF7 cells and a decrease in the mRNA for the antiapoptotic gene *Bcl-2* is detected only in pimozide-treated cells, whereas in mibefradil-treated cells, the toxicity is primarily necrotic; and 3) growth inhibition by mibefradil is reduced in Y79 cells transfected with T-channel antisense and in differentiated Y79 cells (which have decreased T-channel expression), but growth inhibition by pimozide is affected to a lesser extent. These results suggest that pimozide and mibefradil inhibit cell proliferation via different cytotoxic pathways and that in the case of pimozide, it is unlikely that this effect is mediated solely by T-channel inhibition.

Mibefradil and pimozide share several common biological properties, which include Ca^{2+} channel blockage and, in some cell types, inhibition of cell growth. Mibefradil, a benzimidazolyl-substituted tetraline derivative similar in structure to verapamil (Clozel et al., 1990), is distinguished from other Ca^{2+} channel antagonists because it preferentially blocks low-voltage–activated T-type Ca^{2+} channels (T-channels) with 10 to 20 times more selectivity than high-voltage–activated (HVA) L-type Ca^{2+} channels (Mishra and Hermsmeyer, 1994; see Lacinová et al., 2000 for a review). Mibefradil seems to bind to a unique receptor site that overlaps with verapamil and indolizine sulfone sites and is also able to interfere with the binding of Ca^{2+} channel antagonists, such as diltiazem, to dihydropyridine receptors without affecting dihydropyridine binding (Rutledge and Triggle, 1995; Bernink et al., 1996; Glasser, 1998). Mibefradil was introduced clinically in 1997 as an antianginal and antihypertensive agent but was withdrawn from the market less than a year after its release due to potentially life-threatening interactions when mibefradil and β-blockers were taken in combination with, or acutely replaced by, dihydropyridine Ca^{2+} channel blockers (Mullins et al., 1998).

The diphenylbutylpiperidine antipsychotic drug pimozide has also been shown to be a potent inhibitor of T-type Ca^{2+} channels but with less selectivity than mibefradil (Galizzi et al., 1986). In pituitary and heart cells, pimozide inhibits L-type Ca^{2+} channels (Enyeart et al., 1990), whereas in adrenal glomerulosa and spermatogenic cells, it blocks T-channels and Ca^{2+} influx (Enyeart et al., 1993; Arnoult and Florman, 1998). The actions of pimozide and mibefradil are not restricted to Ca^{2+} channels but may also affect other ion channels, including K^+ (Gomora and Enyeart, 1999) and Cl^- channels (Nilius et al., 1997).

Besides their capacity to inhibit T-current, both drugs inhibit the growth of several cell types (Lee and Hait, 1985;

This work was supported by operating grants and salary awards provided by the Canadian Institutes of Health Research, Canadian Breast Cancer Foundation-Atlantic Chapter, and Cancer Research and Education, Nova Scotia. G.E.B. was supported by the Reynolds Fellowship in Pharmacology and a CaRE-Nova Scotia Trainee Award.

ABBREVIATIONS: T-channel, T-type Ca^{2+} channel; DMEM, Dulbecco's modified Eagle's medium; DMSO, dimethyl sulfoxide; PI, propidium iodide; HVA, high-voltage–activated; T-current, T-type Ca^{2+} channel current; RT, reverse transcription; PCR, polymerase chain reaction; bp, base pair(s).

Strobl et al., 1990; Schmitt et al., 1995, 1998). However, the functional role of T-channels in cell growth and the pharmacological properties of these compounds as antiproliferative drugs remain unclear. Recently, it was shown that in cells overexpressing cloned T-channels, there was no alteration in the cell-doubling population time (Chemin et al., 2000), although it has been proposed that the inhibition of smooth muscle proliferation and neointima formation by mibefradil is due to its effect on T-channels (Schmitt et al., 1995). Pimozide has been shown to inhibit tumor cell growth of astrocytoma cells, and the apparent mechanism of action may be via inhibition of calmodulin activity (Lee and Hait, 1985). In breast cancer epithelial cells, the antiproliferative activity of pimozide was thought to be associated with its σ-2–binding capability (Strobl et al., 1998). In addition to actions on Ca^{2+} and K^+ channels, other studies documenting the antiproliferative activity of mibefradil on endothelial cells have also suggested that the effect of this drug could be associated with actions on Cl^- channels (Nilius et al., 1997).

T-type Ca^{2+} channels are the predominant Ca^{2+} channel expressed in mitogenic Y79 cells and the WERI-Rb1 retinoblastoma cell lines that are derived from human retinoblastoma tumors. The cells arise from a primitive neuroectodermal cell and retain the capability to differentiate to neuron or glia-like cells (Kyritsis et al., 1984). Recently, we demonstrated that T-current and mRNA expression of T-channel genes is diminished when Y79 retinoblastoma cells are induced to exit the cell cycle and differentiate (Hirooka et al., 2002). This suggests that T-channels may be important in membrane potential changes and alterations in Ca^{2+} that occur during proliferation and differentiation of Y79 retinoblastoma cells.

In the present study, we examined the growth-inhibitory actions of the Ca^{2+} channel blockers pimozide and mibefradil in inhibiting cell growth in Y79 and WERI-Rb1 retinoblastoma cells and compared results with those of MCF7 breast cancer epithelial cells and C6 glioma cells, two cell lines in which pimozide has been previously demonstrated to inhibit cell proliferation (Lee and Hait, 1985; Strobl et al., 1990, 1998). Our studies examined whether mibefradil and pimozide share common cytotoxic mechanisms and whether the observed antiproliferative actions of these agents might involve T-channel inhibition.

Materials and Methods

Cell Culture. Y79 and WERI-Rb1 (human retinoblastoma), MCF7 (human breast cancer epithelial), and rat glioma C6 cell lines were maintained in Dulbecco's modified Eagle's medium (DMEM) (Sigma-Aldrich, St. Louis, MO) plus 0.02% glutamine supplemented with 10% fetal bovine serum (Invitrogen, Burlington, ON, Canada), without antibiotics. The cells were kept in a humidified 5% CO_2-air atmosphere at 37°C, and the medium was changed twice a week.

Chemical differentiation of Y79 cells was performed in 96-well plastic culture dishes. The dishes were pretreated with poly-D-lysine (100 μg/ml) at room temperature for 6 min, washed once with DMEM, and coated with laminin (10 μg/ml) at 37°C for 30 min. The cells were then rinsed with DMEM and incubated with DMEM plus N2 neuronal supplement (insulin, progesterone, transferrin, selenium, and putrescine; Invitrogen) (Albini et al., 1992). This method yielded approximately 70 to 80% differentiated neuronal-like cells.

Pimozide (Sigma-Aldrich), mibefradil (Hoffman-La Roche, Nutley, NJ), and nifedipine (ICN Pharmaceuticals Biochemicals Division, Aurora, OH) were dissolved in dimethyl sulfoxide (DMSO) and diluted to final concentrations in culture medium. Control cells were exposed to the same concentrations of DMSO, which never exceeded 0.05%.

For cell transfection, Y79 cells were transfected with antisense (nucleotide 2084-2103; GenBank accession no. AF126966) or scrambled fluorescein isothiocyanate-labeled thio-protected oligonucleotides against α1G (Bijlenga et al., 2000). Cells (3–4 $\times$ 10^6 cells/ml) were transfected in serum-free DMEM using Lipofectin (Invitrogen) in the presence of 10 μg of the oligonucleotides according to the manufacturer's protocol. After incubation with Lipofectin, the cells were cytocentrifuged, resuspended, and maintained in growth medium for 48 h before measuring T-current and cell growth. Only cells fluorescing as a result of the presence of the fluorescein isothiocyanate-labeled oligonucleotide were chosen for T-current measurements. The transfection efficiency was approximately 50%.

Measurement of Cell Growth Inhibition and Cytotoxicity. Cell proliferation was quantified using the Cell Titer 96 AQ One Solution Cell Proliferation Assay Kit (Promega, Madison, WI). Cells were plated at 1×10^4 cells/well in 96-well culture plates and treated with different concentrations of pimozide, mibefradil, and nifedipine. The quantity of formazan product formed, which is directly proportional to the number of viable cells, was measured on an enzyme-linked immunosorbent assay reader at 490 nm and converted to cell numbers using a standard curve with different numbers of cells ranging from 1×10^3 to 5×10^4 cells/well.

To measure apoptosis, cytocentrifuged Y79 cells or monolayer cultures for MCF7 cells were stained with a solution composed of acridine orange (100 μg/ml) and ethidium bromide (100 μg/ml) in phosphate-buffered saline (Giuliano et al., 1998). Viable (fluoresce green), necrotic (fluoresce orange), and apoptotic (fluoresce orange with nuclei condensed and pyknotic) cells were visualized under a fluorescent microscope with filters appropriate for fluorescein (495-nm primary filter and 515-nm secondary filter). The percentage of viable, apoptotic, and necrotic cells after pimozide and mibefradil treatment was calculated and analyzed after counting by a person blind to the treatment.

Measurement of Cell Cycle. Cellular DNA content was determined by fluorescence measurement of propidium iodide (PI)-stained cells in a FACScan (BD Biosciences, San Jose, CA). Y79 retinoblastoma cells were treated with 1 M of pimozide or mibefradil for 24 h. Cell were then harvested and fixed in 70% ethanol for 2 h. Subsequently, the fixed cells were incubated in a solution of Ca^{2+}- and Mg^{2+}-free phosphate-buffered saline containing 50 μg/ml RNase A and 200 μg/ml propidium iodide for 1 h. For each cell population, 1×10^4 cells were counted, and the proportions that were in G_0/G_1, G_2/M, and S phases were analyzed using the FCS Express program (De Novo Software, Thornhill, ON, Canada).

RT-PCR. Total RNA was obtained from cells using TRIzol (Invitrogen) according to the manufacturer's protocol. Dnase I-treated RNA samples (2-μg) were used to generate single-stranded cDNA with a mouse mammary tumor virus reverse transcriptase kit (Invitrogen). All PCR amplifications were carried out in a total volume of 25 μl with 200 ng of cDNA, 400 nM primers, 50 mM KCl, 10 mM Tris-HCl, pH 8.0, 1.5 mM $MgCl_2$, 200 μM dNTP, and 1.25 units of recombinant *Taq* polymerase (MBI Fermentas, Burlington, ON, Canada). Primer sequences have been published previously for α1G, α1H, and cyclophylin (Hirooka et al., 2002), Bax and *Bcl-2* (Wang and Phang, 1995), cyclin A (Maas et al., 1995), and cyclins D (D1, D2, and D3; Sola et al., 1999). To compare the mRNA expression level between treated and untreated cells, the number of PCR cycles was determined to be within the linear range. The number of PCR cycles and the annealing temperature for each gene analyzed was 1) α1G and α1H, 33 cycles at 63°C; 2) cyclophilin, 26 cycles at 50°C; 3) Bax and *Bcl-2*, 31 and 35 cycles, respectively, at 65°C; and 4) cyclins D1, D2, and D3 together and cyclin A, 35 and 24 cycles, respectively, at 51°C.

The PCR products were fractioned by agarose gel electrophoresis

(1.5%), and the ethidium bromide emission was visualized under UV illumination using a Geldoc apparatus (Bio-Rad, Mississauga, ON, Canada). The images of the PCR product bands were analyzed semi-quantitatively using Molecular Analyst image analysis software version 1.5 (Bio-Rad, Hercules, CA).

Electrophysiology. Whole-cell voltage-clamp recordings were made from Y79, WERI-Rb1, glioma C6, and MCF7 cells. For recording, cells were plated on glass coverslips, placed in a 1-ml experimental chamber, and continuously superfused with external solutions. For T-current recordings, the cells were superfused with bath solution containing 150 mM NaCl, 5 mM KCl, 1.5 mM $CaCl_2$, 20 mM $BaCl_2$, 1 mM $MgCl_2$, 5 mM glucose, and 5 mM HEPES, pH 7.4. The patch pipette contained 155 mM CsCl, 5 mM HEPES, and 1 mM EGTA, pH 7.2. In some recordings of MCF7 cells, 1 mM EGTA was replaced with 5 mM EGTA in the internal pipette solution. All recordings were made at room temperature (21–24°C). Pimozide and mibefradil were made as stocks in DMSO, dissolved in external solutions, and superfused at concentrations cited under *Results*. In all cases, the final DMSO concentration did not exceed 0.1%, a concentration previously shown not to affect Ca^{2+} currents (Hirooka et al., 2000).

Whole-cell patch-clamp recording techniques were used to measure currents in isolated cells. Patch electrodes were pulled from 1.1 to 1.2- (inside) and 1.3 to 1.4-mM (outside) diameter capillary glass (15401-659; VWR International, West Chester, PA) on a two-stage pipette puller (KOPF model 730; David Kopf Instruments, Tujunga, CA). Electrodes had a 2.5 to 6 MΩ resistance when filled with internal solutions. The bath solution was connected to the Ag/AgCl bath electrode by a 1% agar bridge.

Membrane potential and currents were recorded with an Axopatch 1-D amplifier (Axon Instruments, Inc., Union City, CA). Signals were filtered at 2 kHz (−3-db, 4-pole Bessel filter) and digitized at 4 kHz using an Indec Systems interface (Indec Systems, Inc., Capitola, CA) directly to a PC-compatible computer. Stimulus generation, data acquisition, and plotting were controlled by BASIC-FASTLAB program software (Indec Systems). Before seals were made on cells, offset potentials were nulled using the amplifier circuitry. Capacitance subtraction and series resistance compensation was used in all recordings.

Statistical Analysis. All data are presented as mean ± S.E.M. unless otherwise stated. The statistical methods used were repeated-measures analysis of variance and two-tailed Student's t test for unpaired data, when appropriate. $p < 0.05$ was considered statistically acceptable.

Results

Pimozide and Mibefradil Inhibit Cell Growth. To examine the effect of the pimozide and mibefradil on growth of retinoblastoma cells and compare this with MCF7 and C6 glioma cells, we first estimated the population-doubling time of each cell line. Retinoblastoma Y79 and WERI-Rb-1 cells showed similar duplication time in the log phase, which was approximately 50 to 60 h, whereas glioma C6 and MCF7 had a shorter time (30–36 h; data not shown). Thus, the effect of the compounds was tested at times corresponding to approximately half of the duplication time for each cell line (24–28 h for retinoblastoma cells and 16–18 h for glioma C6 and MCF7 cells).

Figure 1, A and B, shows that mibefradil and pimozide inhibited retinoblastoma cell proliferation in a dose-dependent manner. The IC_{50} values for the Y79 cell line were 0.9 ± 0.2 (n = 8) and 1.2 ± 0.4 μM (n = 8) for pimozide and mibefradil, respectively (Fig. 1A). Similar antiproliferative activity was observed with both drugs when tested on WERI-Rb-1 cells. The IC_{50} for pimozide was 1.2 ± 0.6 (n = 6) and for mibefradil was 1.5 ± 0.5 μM (n = 6) (Fig. 1B). Mibefradil and pimozide also inhibited the proliferation of glioma C6 cells, although at higher doses than that required for retinoblastoma cells. For C6 cells, the IC_{50} for pimozide was 8.0 ± 2.1 (n = 4), which is consistent with previously reported values

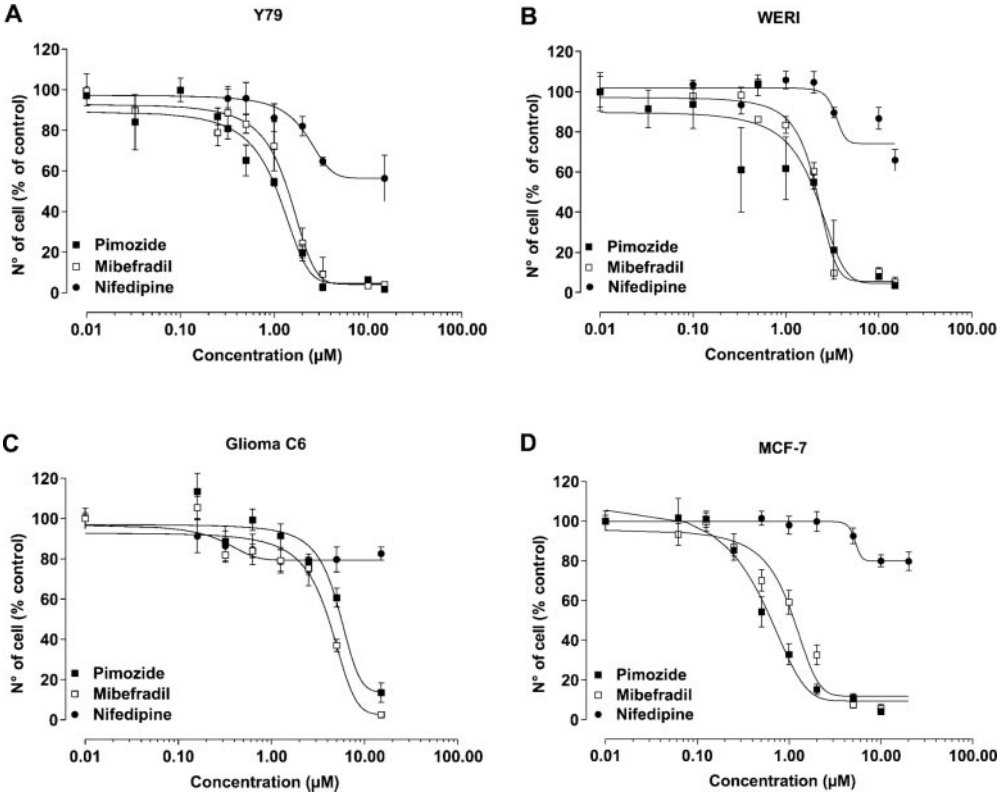

Fig. 1. Growth-inhibition curves for pimozide, mibefradil, and nifedipine in Y79 retinoblastoma (A), WERI-Rb1 retinoblastoma (B), glioma C6 (C), and breast cancer epithelial MCF7 cells (D). The number of live cells, measured as described under *Materials and Methods*, was normalized with respect to control (100%) and plotted against drug concentrations. Values shown are mean ± S.E.M. Solid lines, dose-response curves fit to each data set and given by the equation: $y = (m / 100 - m) / (1 + 10^{(\log IC_{50} - c) \times n_H})$, where m is the minimum percentage of viable cells for each data set, c is the concentration of drug, and n_H is the Hill coefficient.

(10 μM; Lee and Hait, 1985), whereas the IC_{50} we obtained for inhibition of C6 growth by mibefradil was 5.0 $\pm$ 1.0 μM ($n = 4$) (Fig. 1C). In MCF7 cells, the IC_{50} values for inhibition of proliferation by pimozide and mibefradil were 0.6 $\pm$ 0.1 ($n = 6$) and 1.1 $\pm$ 0.2 μM ($n = 6$), respectively. The IC_{50} values in MCF7 cells are similar to values previously reported for pimozide inhibition in these cells (0.6–3 μM; Strobl et al., 1990, 1998) and similar to the values we obtained in retinoblastoma cells (pimozide, $p > 0.05$; mibefradil, $p > 0.05$) but are significantly lower than the IC_{50} values we obtained in glioma C6 cells (pimozide, $p < 0.001$; mibefradil, $p < 0.001$).

We also examined whether other Ca^{2+} channel blockers, such as the L-type Ca^{2+} channel blocker nifedipine, could inhibit proliferation of retinoblastoma cells. Undifferentiated retinoblastoma cells express very little HVA current relative to T-current (Hirooka et al., 2002). Dose-response assays for growth inhibition in retinoblastoma, C6 glioma, and MCF7 cells demonstrated that nifedipine did not exhibit a significant growth inhibitory effect and only inhibited 20 to 40% of the cell proliferation at the maximum concentration tested (15–20 μM) in all four cell lines (Fig. 1, A-C), possibly reflecting T-channel block or other nonspecific effects.

We further investigated whether the growth inhibition observed with pimozide and mibefradil in retinoblastoma and MCF7 cells could be additive or synergistic. In the case of common mechanisms/pathways of inhibition, the antiproliferative effect of pimozide and mibefradil should be additive, and the cell growth inhibition in the presence of both drugs should be close to the sum of the levels measured for pimozide and mibefradil alone. On the other hand, if the drugs act by similar and/or independent pathways to produce growth inhibition, then a synergistic effect would be expected.

Figure 2A shows growth inhibition curves for Y79 cells in the presence of pimozide and mibefradil alone or when the two drugs were combined. Inhibition when the drugs were

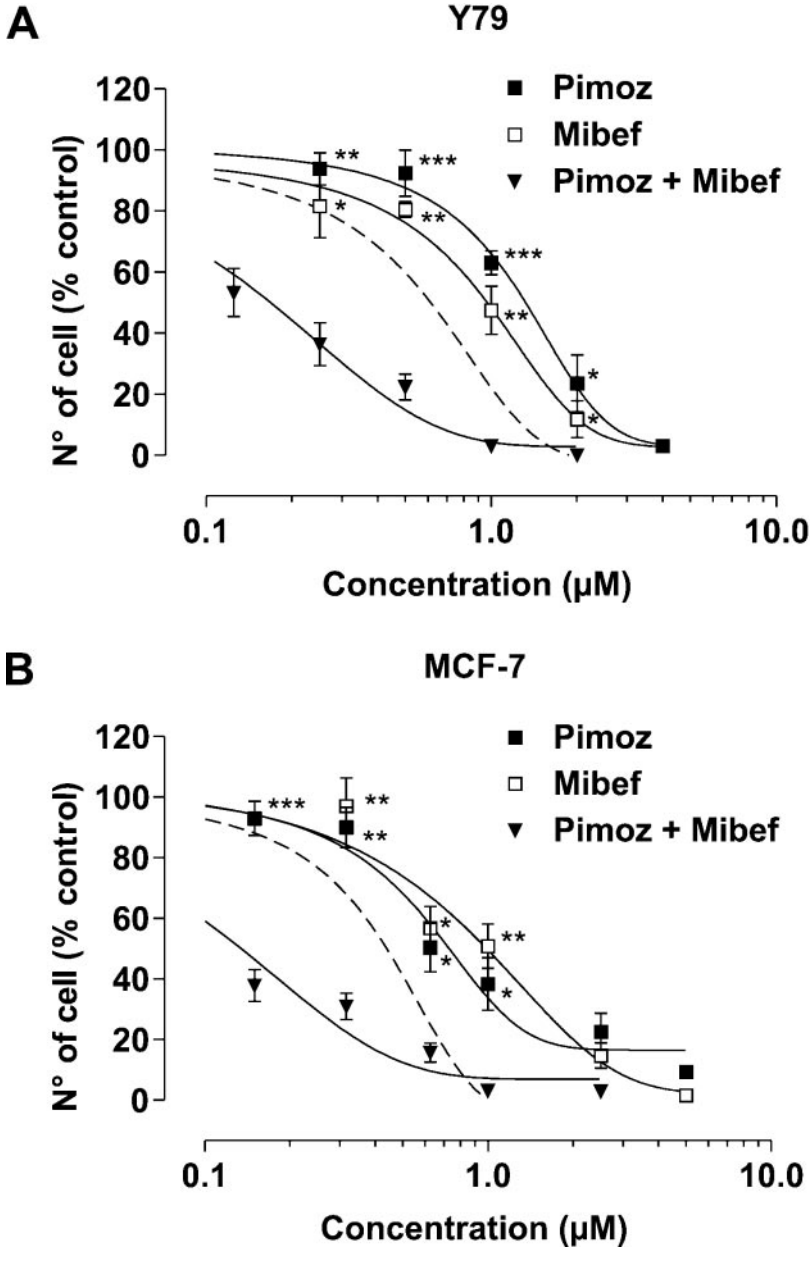

Fig. 2. Synergy in cell growth inhibition by pimozide and mibefradil in Y79 retinoblastoma (A) and breast cancer epithelial MCF7 cells (B). Cell growth inhibition was measured as described in Fig. 1. Solid lines, dose-response curves fit to each data set as described in Fig. 1. Dashed lines, theoretical dose-response curves that would be obtained if the drugs had purely additive effects. ⋆, significance of the difference between the drugs combined and alone at $p < 0.05$, $p < 0.01$, and $p < 0.001$ levels. A, there was no difference between pimozide and mibefradil alone at any concentration ($p > 0.05$). At 0.25 μM, the combination differed significantly from pimozide and mibefradil alone ($p < 0.01$ and $p < 0.05$, respectively). At 0.5 and 1 μM, the combination differed significantly from pimozide and mibefradil alone ($p < 0.001$ and $p < 0.01$, respectively, both concentrations). B, there was no difference between pimozide and mibefradil alone at any concentration ($p > 0.05$). At 0.15 μM, the combination differed significantly from pimozide and mibefradil alone ($p < 0.001$ for both). At 0.32 μM, the combination differed significantly from pimozide and mibefradil alone ($p < 0.01$ for both). At 0.62 μM, the combination differed significantly from pimozide and mibefradil alone ($p < 0.05$ for both). At 1 μM, the combination differed significantly from pimozide and mibefradil alone ($p < 0.05$ and $p < 0.01$, respectively).

combined was much greater than the theoretical additive effects, which are shown in the dashed line. At combined concentrations for pimozide and mibefradil of 0.25, 0.5, and 1 μM each, the block was significantly greater than when drugs were applied alone.

Similar results were observed in MCF7 cells (Fig. 2B), where growth inhibition with the drugs combined was also much greater than when either drug was added alone. These results suggest that different mechanisms are involved in the antiproliferative activity of pimozide and mibefradil.

Cytostatic or Cytotoxic Effects of Pimozide and Mibefradil. Inhibition of cell growth may be attributed, at least in part, to arrest of cells in a specific phase of the cell cycle. To determine whether pimozide and mibefradil could produce alterations in cell cycle regulation, we investigated whether either of the drugs could inhibit the proliferation of Y79 cells by arresting and/or killing cells in a specific phase of the cell cycle. Figure 3A shows the cell cycle analysis of PI-stained cells using a FACScan. Unsynchronized Y79 cells seeded at a density $>1 \times 10^6$ cell/ml were counted after 24 h of incubation with 1.5 μM pimozide and mibefradil. The percentage of control cells in G_0/G_1, S, and G_2/M phase was 46.8 $\pm$ 2.9, 15.9 $\pm$ 1.0, and 37.2 $\pm$ 2.9% ($n = 3$), respectively. Similar percentages were obtained in the same cell cycle phases in pimozide- and mibefradil-treated cells with 45.8 $\pm$ 3.9, 15.9 $\pm$ 3.6, and 38.2 $\pm$ 5.6% of cells in G_0/G_1, S, and G_2/M phase in the mibefradil-treated group and 49.0 $\pm$ 2.8, 13.7 $\pm$ 1.0, and 37.2 $\pm$ 2.5% in the pimozide-treated groups, respectively ($n = 3$).

We also examined the expression of cyclin D family (D1, D2, and D3) and cyclin A in pimozide- and mibefradil-treated cells. D cyclins form complexes with the regulatory proteins cdk4 and cdk6 and modulate the expression of genes involved in proliferation during the G_1 phase. Cyclin A associates with cdk2 during S phase and with cdk1 at the S-G_2 boundary and into G_2 phase. Both have a central role in controlling cell cycle progression, and their expression during the cell cycle is tightly regulated (Guttridge et al., 1999). We obtained PCR products for all D cyclins and cyclin A in Y79 retinoblastoma cells using cDNA from undifferentiated Y79 cells as a template. However, expression of product for cyclin D1 (428 bp) was lower than cyclins D2 (353 bp) and D3 (243 bp), and its detection required increased PCR cycles saturating the densitometric detection for semiquantitative analysis of cyclins D2 and D3 (data not shown). Figure 3, B and C, shows RT-PCR and densitometric analysis of cDNA derived from control and drug-treated Y79 cells. The concentrations of pimozide and mibefradil used (1 μM) were similar to those that produced 50% growth inhibition in the cell proliferation assays. A constitutive housekeeping gene, cyclophilin, was used as an internal control for PCR reactions and produced a 371-bp PCR product. No significant changes in cyclins D1, D2, or D3 and cyclin A expression were detected after 8 h of treatment with pimozide and mibefradil. Similar findings for cyclin expression were obtained in three other experiments. These results, together with the flow cytometry results, suggest that pimozide and mibefradil exert their growth-inhibitory effects on retinoblastoma cells via mechanisms independent of cell cycle alterations.

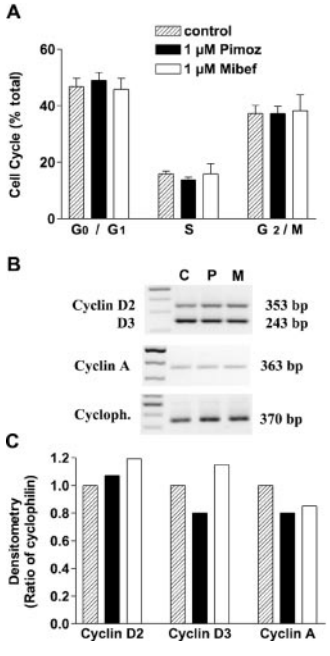

Fig. 3. Effects of pimozide and mibefradil on Y79 cell cycle. A, flow cytometry analysis of Y79 cells stained with PI after 24 h of treatment with 1 μM pimozide or mibefradil or no drug (control). Percentage of cells in G_0/G_1, S, and G_2/M (mean $\pm$ S.E.M.) in three independent experiments are shown. B, RT-PCR for cyclins D2, D3, and A and cyclophilin in Y79 retinoblastoma cells treated for 8 h with 1 μM pimozide (P) or mibefradil (M) or no drug (C). C, densitometric analysis for PCR results shown in B. Values were normalized against the density of cyclophilin.

Previous studies have suggested that the antiproliferative actions of pimozide may be attributed to the initiation of apoptotic cell death pathways (Strobl et al., 1998). Further experiments using a cell viability assay with acridine orange and ethidium bromide examined the cytotoxic actions of pimozide and mibefradil in retinoblastoma cells and compared this with untreated control cells. In this assay, dead cells stain orange, and viable cells appear green. Apoptotic and necrotic cells are distinguished by morphological changes (Giuliano et al., 1998). Figure 4A shows fluorescent photomicrographs of stained cells in control (C), 1.0 μM pimozide (P)-treated, and 1 μM mibefradil (M)-treated groups. Control cell groups consisted of primarily of viable cells, which exhibited green fluorescence (Fig. 4A, left). In the pimozide group, a number of apoptotic cells, small cells with condensed fluorescent orange nuclei, often with yellow shift color, are apparent (Fig. 4A, middle). In the mibefradil group, cells appeared necrotic with evidence of cell swelling and both cytoplasmic and nuclear orange fluorescence (Fig. 4A, right). Mean data from cell viability assays are shown in Fig. 4B. In control groups, approximately 85 to 90% of the cells were viable, whereas the rest (10–15%) showed a similar number of necrotic and apoptotic cells. Three-fold more dead cells (30–40%) were observed in cells treated with pimozide. This was due almost exclusively to the higher number of apoptotic cells present in the pimozide-treated group. In contrast, the increased cell death (30–40%) in mibefradil-treated cultures seemed to be attributable to an increase (30%) in necrotic cells.

The effects of pimozide and mibefradil in producing apoptotic versus necrotic effects were further analyzed by examining mRNA expression of the genes *Bcl-2* and Bax after 8 h of treatment with pimozide and mibefradil (1.0 μM). Decreased levels of *Bcl-2* protein are normally associated with apoptosis in response to external stimuli. The antiapoptotic

activity of *Bcl-2* is modulated by Bax, and increased levels of Bax have been reported for cells undergoing apoptosis (for a review see Adams and Cory, 2001). Figure 4, C and D, shows RT-PCR and densitometry analysis for Bax and *Bcl-2* in Y79 retinoblastoma cells after pimozide and treatment. A decrease in *Bcl-2* mRNA expression was only detected in pimozide-treated cells. No significant change in *Bcl-2* was observed in mibefradil-treated cells, and no effect in Bax mRNA expression was detected after 8 h of treatment with either pimozide or mibefradil. Similar findings were obtained in two other experiments. These results support the cell viability assays and suggest that the growth-inhibitory actions of pimozide in retinoblastoma cells occur via activation of apoptotic pathways of cell death, whereas the cytotoxic actions of mibefradil may occur via different mechanisms that result primarily in necrotic loss of cells.

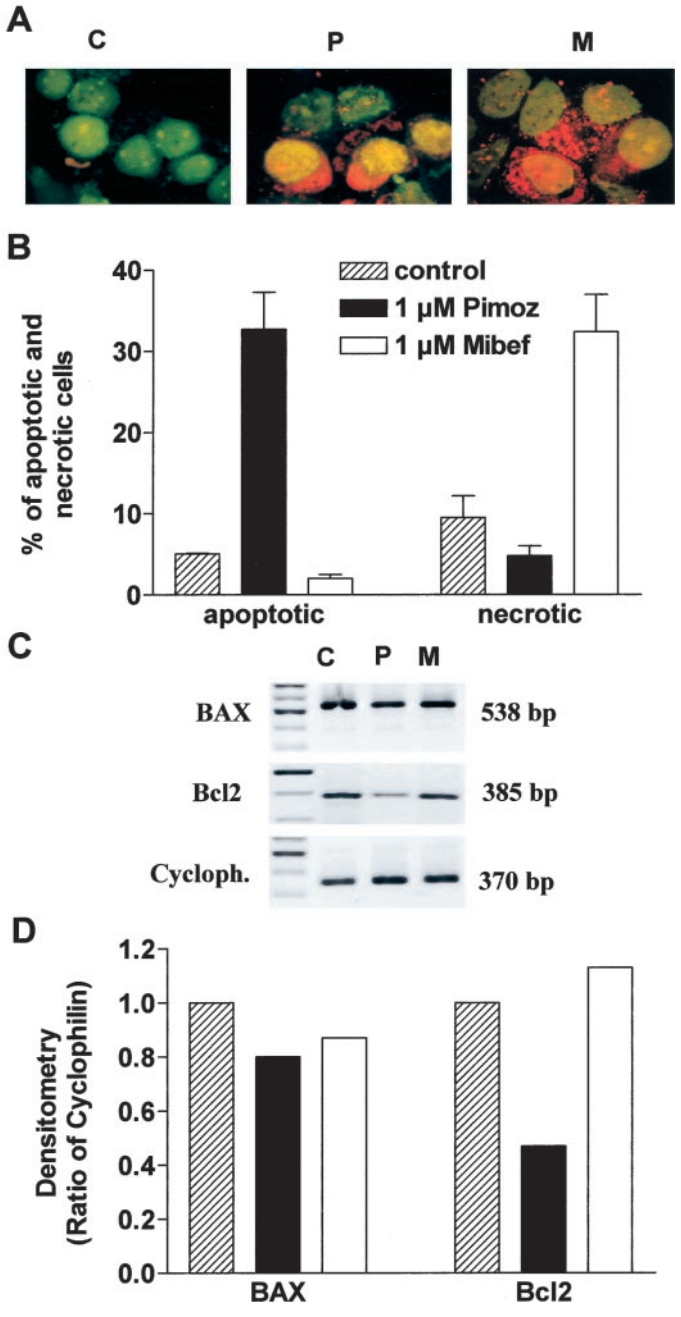

Fig. 4. Induction of apoptosis and necrosis by pimozide and mibefradil in Y79 cells. A, Y79 cells treated with no drug (C) or 1.5 μM pimozide (P) or mibefradil (M). Cells were cytocentrifuged and stained with acridine orange (100 μg/ml)-ethidium bromide (100 μg/ml) staining solution. The cell bodies are approximately 10 μm in diameter. B, the number of apoptotic and necrotic cells expressed as percentage of the total in control (C), pimozide (P)-, and mibefradil (M)-treated groups. C, RT-PCR of BAX, *Bcl-2*, and cyclophilin in Y79 cells treated for 8 h with 1 μM pimozide or mibefradil. The expected PCR product and the corresponding densitometric values are normalized against the density of cyclophilin.

T-Channel Expression and Effects of Pimozide and Mibefradil. We examined whether the growth-inhibitory effect of pimozide and mibefradil could be accounted for, at least in part, by block of T-channels. We first confirmed the presence of T-channels using RT-PCR with primers specific for α1G and α1H Ca^{2+} channel subunit RNA, using cDNA derived from undifferentiated cycling Y79 or WERI-Rb1 cells, and compared this with product obtained with cDNA from differentiated retinoblastoma cells that had been growing on a poly-D-lysine/laminin substrate for 6 to 12 days in defined medium. Under these conditions, retinoblastoma differentiated primarily into a neuronal phenotype. Because both drugs also inhibited cell growth in C6 glioma cells and MCF7 cells, we also determined whether T-channels were expressed in these cell lines. Figure 5A shows that, in accordance with our previous findings in Hirooka et al. (2002), undifferentiated retinoblastoma cells (Y79U) and WERI-Rb1 retinoblastoma cells have mRNA for both α1H (435-bp) and α1G (395-bp) T-type Ca^{2+} channels, the expression of which was decreased on exit of cells from the cell cycle and differentiation into a neuronal phenotype (Y79D). Under the conditions used, glioma C6 cells failed to shown any discernible PCR product for either α1H or α1G T-channels, and patch-clamp recordings from these cells did not detect measurable T-current (data not shown). PCR product was obtained for both α1H and α1G T-channels in MCF7 cells (Fig. 5B).

Confirmation of the presence of T-channels in MCF7 cells was provided by whole-cell patch-clamp recording. Figure 5C shows whole-cell currents recorded from MCF7 cells using Ba^{2+} as a charge carrier. Transient inward T-type Ca^{2+} channel current was apparent when the membrane voltage was stepped from -80 mV to potentials positive to -60 mV. Figure 5D shows mean current-voltage relations from 16 cells. Inward current activates at -50 mV, with peak current at -10 mV. The amplitude of T-current in MCF7 cells varied between 10 and 168 pA ($n = 16$), and the mean T-current density determined in a subset of cells was 0.80 ± 0.35 pA/pF ($n = 5$), which is substantially less than current density previously reported in retinoblastoma cells under the same conditions (5.9 ± 1.1 pA/pF; Hirooka et al., 2002). Mean values for T-current block by mibefradil and pimozide in MCF7 cells (Fig. 5E), however, were similar to those found in retinoblastoma (Hirooka et al., 2002), with approximately 50% of T-current activated at -10 mV inhibited by both mibefradil and pimozide at 1 μM. Current was almost completely inhibited (>75%) at 5 μM. These values are also consistent with IC_{50} values for growth inhibition in retinoblastoma and MCF7 cells by pimozide and mibefradil. In C6 glioma cells in which we were unable to detect T-current, both mibefradil and pimozide required 10-fold higher concentrations to produce growth inhibition. Normalized, mean current-voltage plots for MCF7 cells treated with 1 and 5 μM of mibefradil revealed that although current inhibition was observed at all the voltages tested, T-current inhibition by

mibefradil was increased at more positive voltages, and a shift was observed in the current-voltage relationships to more negative potentials (Fig. 5F).

We next examined whether the blocking effects of pimozide and mibefradil on T-currents in Y79 retinoblastoma cells were synergistic, as determined for the antiproliferative actions of these agents. Pimozide and mibefradil were administered alone and in combination to determine the degree to which inhibition of T-currents occurred. Figure 6A shows that pimozide and mibefradil alone blocked the T-current with IC_{50} values of 0.83 and 0.60 μM, respectively. In contrast to the synergy in cell growth inhibition, combined administration of the drugs produced only additive inhibition of T-current.

We investigated whether down-regulation of T-channels by antisense transfection could lead to detectable changes in growth-inhibitory effects mediated by pimozide and mibefradil. Our whole-cell patch-clamp recordings from Y79 cells transfected with antisense oligonucleotides against α1G T-channels revealed a >70% reduction in T-current, suggesting that α1G T-type Ca^{2+} channels may be the most abundant T-channel in retinoblastoma cells. Figure 6B shows mean T-current recorded at −10 pA in antisense-transfected cells (42 ± 8 pA, n = 11) compared with T-current recorded in sense-transfected (107 ± 20 pA, n = 11) or control cells (105 ± 19 pA, n = 10), respectively. Figure 6C shows that cells transfected with α1G antisense oligonucleotide were less sensitive to the growth inhibition mediated by mibefradil than sense-transfected and control cells. The inhibitory effect produced by pimozide seemed to be similar in control, sense, and antisense transfected cells, suggesting that in contrast to mibefradil, inhibition of T-channels is not essential for the cytotoxic actions of pimozide.

A test of this result was obtained by comparing the growth inhibition of both mibefradil and pimozide in undifferentiated cycling retinoblastoma cells and differentiated noncycling retinoblastoma cells, in which T-channel expression and T-current is decreased (see Fig. 5A). The cytotoxic effects of

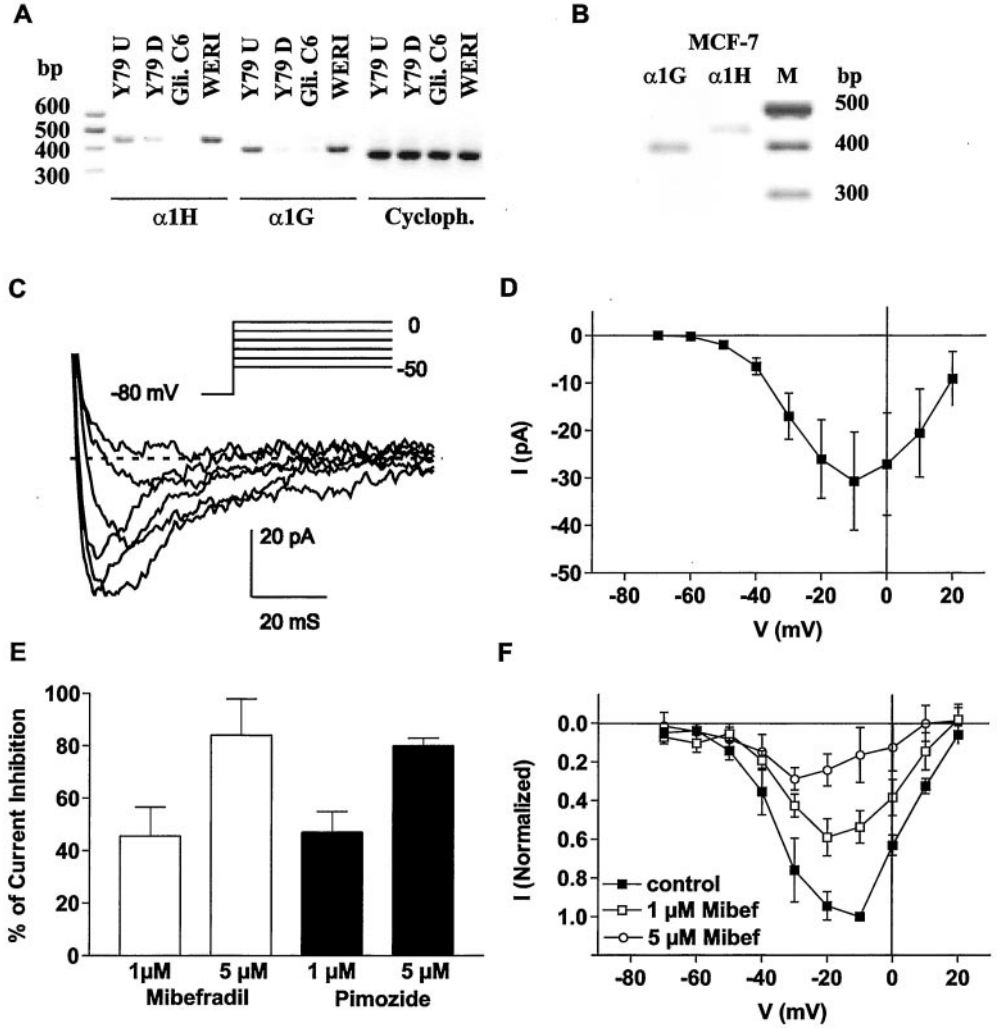

Fig. 5. Expression and pharmacology of T-type Ca^{2+} channels in the cell lines. A, RT-PCR of the T-type Ca^{2+} channel α1 subunits, α1G (395 bp) and α1H (435 bp), and cyclophilin (370 bp) in undifferentiated (Y79U) and differentiated Y79 (Y79D), glioma C6 (Gli C6), and retinoblastoma WERI-Rb1 cells (WERI). B, RT-PCR of the T-type Ca^{2+} α1 subunits and cyclophilin in MCF7 cells. C, T-type Ca^{2+} channel currents recorded in MCF7 cells under voltage clamp during steps between −50 and 0 mV from a holding potential of −80 mV. Dashed line, zero current. D, average current-voltage relationship of T-type Ca^{2+} channel current in MCF7 cells (mean ± S.E.M., n = 16). Capacitance of these cells varied between 41 and >100 pF and was not correlated with current magnitude. E, inhibition of the T-type Ca^{2+} channel current in MCF7 cells by 1 and 5 μM concentrations of mibefradil and pimozide. The currents were recorded during a step to −10 mV from a holding potential of −80 mV. F, normalized mean current-voltage relationship of MCF7 cells in control and in the presence of mibefradil at 1 and 5 μM.

pimozide and mibefradil (5 μM) were examined on both undifferentiated and differentiated cells after 24 h of drug treatment. Figure 6D shows that, as observed in the α1G antisense-transfected retinoblastoma cells, the number of differentiated retinoblastoma cells diminished by only 40% with mibefradil treatment compared with approximately 80% in the undifferentiated retinoblastoma cell cultures. The growth inhibitory-effect of pimozide, however, was similar in both undifferentiated (89 ± 5% reduction in cell number) and differentiated (83 ± 8% reduction in cell number) retinoblastoma cells (Fig. 6D).

Discussion

We observed that the T-channel–blocking drugs pimozide and mibefradil have potent dose-dependent antiproliferative and cytotoxic effects in retinoblastoma and MCF7 cells. The 50% growth inhibition for these drugs occurred at concentrations between 0.6 and 1.5 μM and at lower doses when mibefradil and pimozide were combined to produce synergistic growth inhibition. Examination of the cytotoxic effects of these drugs suggested that mibefradil and pimozide produced cell death via different mechanisms independent of alterations in cell cycle regulation. Pimozide-treated cells underwent apoptosis, whereas mibefradil-treated cells appeared to undergo necrosis.

A common role for T-channels in the antiproliferative effect of these drugs was suggested by the good correlation between 50% T-current inhibition and the growth inhibition produced by pimozide and mibefradil in undifferentiated Y79 cells and

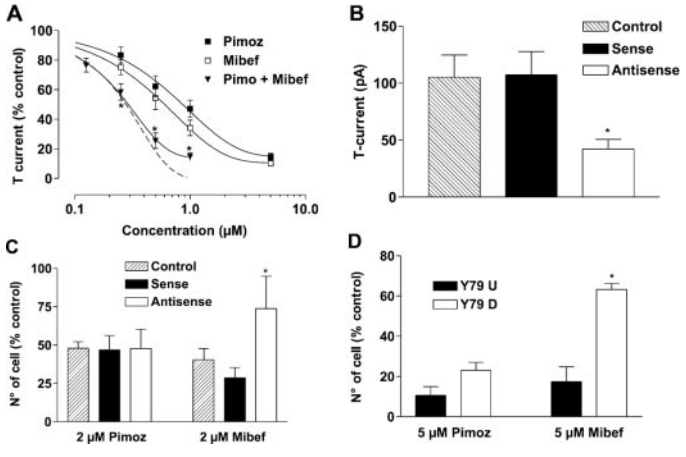

Fig. 6. A, inhibition of T-type Ca^{2+} channel currents in undifferentiated Y79 cells by pimozide, mibefradil, or both drugs combined. Solid lines, dose-response curves fit to each data set (as described in Fig. 1 and with values given in text). Dashed line, theoretical dose-response curve that would be obtained if the drugs had purely additive effects. Only the combined drug effect relative to that of pimozide was significant at the $p < 0.05$ level (indicated by ⋆). The currents were recorded during steps to −10mV from a holding potential of −80 mV. B, T-type Ca^{2+} channel currents recorded in Y79 cells (control) or 48 h after transfection with antisense or sense oligonucleotides against α1G T-type Ca^{2+} channel subunits. The mean current ± S.E.M. ($n = 10$) is shown. ⋆, $p < 0.01$. Cell capacitances ranged between 13 and 15 pF in undifferentiated retinoblastoma cells. C, inhibition of cell growth by 2 μM concentrations of pimozide and mibefradil in undifferentiated Y79 cells (control) and in cells transfected with either antisense or sense oligonucleotides against the α1G Ca^{2+} channel subunit. The cells were treated with the drugs for 24 and 48 h after transfection. D, cell growth inhibition by 5 μM each pimozide and mibefradil in undifferentiated (Y79U) and differentiated (Y79D) Y79 cells. Data are expressed as the mean ± S.D. ($n = 3$) and were normalized against untreated cells (C and D).

MCF7 epithelial cells at 1 μM. However, several findings also supported distinct mechanisms of cytotoxicity for both mibefradil and pimozide. In the case of pimozide, these seemed to be independent of T-channel inhibition. First, cell growth inhibition in Y79 cells with concomitant administration of both drugs was synergistic, but T-current inhibition was additive. Second, retinoblastoma cells with α1G T-channel knockdown by antisense oligonucleotide transfection were less sensitive to growth inhibition by mibefradil but not pimozide. Third, differentiated retinoblastoma cells with diminished T-current and with low expression of mRNA for both the T-type Ca^{2+} channels α1G and α1H were less sensitive to the growth inhibition mediated by mibefradil but not to pimozide. Taken together, these data suggest that pimozide and mibefradil induce cell death in retinoblastoma and MCF7 cells by different pathways. In the case of mibefradil, the mechanism of cell death was primarily necrotic and largely dependent on block of T-channels. However, cell death caused by pimozide seemed to involve apoptosis and did not rely on T-channel block.

Pimozide and Mibefradil: Actions on Cell Proliferation. Pimozide has been reported to inhibit cell proliferation in a number of cell types and cancer cell lines (Lee and Hait, 1985; Strobl et al., 1990). In MCF7 cells, the antiproliferative activity of pimozide was associated with interaction with σ-2 receptors (Strobl et al., 1998). σ-2 receptors are drug-binding proteins that are expressed in high densities in a variety of tumor types (Vilner et al., 1995) and bind structurally distinct psychoactive agents, including various neuropleptic drugs. Investigations of the apoptosis and cytotoxicity associated with σ-2 receptor ligands in MCF7 cells revealed that this was p53-independent and did not seem to be dependent on caspase activation (Crawford and Bowen, 2002). Studies examining the actions of σ-2 agonists in neuroblastoma cells and colon and mammary carcinoma cells demonstrated that ligands that interacted with σ-2 receptors could release Ca^{2+} stores, which triggered subsequent extracellular Ca^{2+} influx after the depletion of the stores. Prolonged exposure to σ ligands resulted in cell death via apoptosis (Brent et al., 1996; Vilner and Bowen, 2000). In C6 glioma cells, the dose-dependent cytotoxic effect of σ ligands was reported to result in receptor-mediated alterations in cellular morphology, cessation of cell division, and inhibition of calmodulin activity (Lee and Hait, 1985; Vilner et al., 1995).

Our data in retinoblastoma and MCF7 cells are in agreement with these findings in that pimozide produced apoptosis with a similar IC_{50} for growth inhibition in both cell lines. Because retinoblastoma cells express caspase 3, whereas MCF7 cells, due to aberrant mRNA splicing, lack caspase 3 (Jänicke et al., 1998), our data would suggest that the pimozide-mediated apoptosis observed was caspase-independent or involved activation of caspases other than caspase 3. The IC_{50} for growth inhibition by pimozide was also in the range of published values for block of T-channels in a number of other cell types. However, in retinoblastoma cells treated with α1G T-channel antisense or in differentiated retinoblastoma cells in which T-channel expression is significantly decreased, the IC_{50} for pimozide cytotoxicity was unchanged. This suggests that although pimozide may block T-channels, this is not the primary mechanism triggering cell death. Synergistic growth inhibition by pimozide with mibefradil, another T-channel–blocking drug, in contrast to additive ac-

tions on T-currents suggests that additional mechanism(s) contribute to the cytotoxicity. This may also include σ-2 receptor activation.

Mibefradil has also been reported to inhibit the proliferation of various cell types, including blood mononuclear cells (Lijnen et al., 1999), rat smooth muscle cells (Schmitt et al., 1995), mouse liver cells (Wondergem et al., 2001), and endothelial cells (Nilius et al., 1997). In hemopoetic cells, the antiproliferative effect of mibefradil involved 1) a decrease in DNA synthesis as defined by decreased [^{3}H]thymidine incorporation and 2) was dependent on the timing of drug administration and involved Ca^{2+} channel block (Lijnen et al., 1999). Mibefradil was reported to prevent neointima formation after vascular injury in rats (Schmitt et al., 1995). This in vivo effect of mibefradil was attributed to inhibition of smooth muscle cell proliferation and to block of T-channels, based on the increased density of T-channels present in the proliferating muscle cells and the lack of effect of other dihydropyridine-type HVA Ca^{2+} antagonists. In liver, endothelial, and neuroblastoma cells, mibefradil was also reported to inhibit cell proliferation, and this was associated with cell swelling and inhibition of volume-sensitive Cl^- channels (Nilius et al., 1997; Rouzaire-Dubois and Dubois, 1998; Wondergem et al., 2001).

Our data examining the actions of mibefradil on retinoblastoma and MCF7 cells are supportive of an involvement of T-channel inhibition in contributing to the cytotoxic actions of this drug; mibefradil inhibited cell growth and T-current at approximately the same concentration, and the actions of mibefradil were reduced in cells treated with α1G antisense or in differentiated retinoblastoma cells with diminished T-channel expression.

T-Channels and the Cell Cycle. Although the biological role of T-channels in cell proliferation has yet to be fully defined, the expression of Ca^{2+} channels has been reported to change with cell differentiation and proliferation. Such changes may contribute to altered membrane excitability during development or regrowth after disease. T-channels seem to be preferentially expressed during development in both neurons and muscle, with a decrease in expression after differentiation (Kuga et al., 1996). In human myoblasts, T-type Ca^{2+} currents are expressed just before fusion, and their inhibition suppresses fusion and the increase in intracellular Ca^{2+} that is normally observed at the onset of fusion (Bijlenga et al., 2000). Re-expression of T-channels has been reported in remodeled hypertrophied ventricular myocytes in which DNA replication is reinitiated in the terminally differentiated phenotype (for review, see Boyden and Jeck, 1995). These alterations in cardiac T-channels coincided with alterations in the cell cycle and suggested that cell cycle changes can regulate expression of T-channels. In aortic smooth muscle cells, expression of T-channels was reported to increase during the cell cycle, appearing in G_1 phase and increasing in the S phase. Nonproliferative muscle cells did not express T-channels (Kuga et al., 1996).

In retinoblastoma cells, α1G and α1H T-channels are the predominant Ca^{2+} channels expressed in cycling, nonspiking undifferentiated cells (Hirooka et al., 2002). Electrophysiological studies have revealed that T-channels in these cells produce "window current" at membrane potentials between -50 and -30 mV (Barnes and Haynes, 1992) and that T-channel activation can lead to regenerative Ca^{2+} spikes (Hirooka et al., 2002). Exit of these cells from the cell cycle and differentiation into a neuronal phenotype is accompanied by loss of T-channels and increased expression of voltage-dependent Na^+ and HVA channels. This suggests a functional role for T-channels in the regulation of membrane excitability during retinoblastoma cell proliferation. However, it should be noted that a recent study noted no significant alterations in the cell proliferation rate in human embryonic kidney cells overexpressing T-channels (Chemin et al., 2000). Although mibefradil was found to diminish calcium influx in overexpressing HEK-293 cells, its effect on proliferation of this cell line was not studied. The authors concluded that although T-channels can mediate increases in intracellular Ca^{2+} and are important in the regulation of basal Ca^{2+} levels, increased expression does not seem to affect either cell proliferation or cell cycle kinetics. Although this study does not eliminate a contribution of T-channels to cell proliferation, it does suggest that these channels are unlikely to be a primary trigger for stimulation of cell cycle progression.

Our experiments examining the antiproliferative and cytotoxic actions of the T-channel–blocking drugs pimozide and mibefradil demonstrate that these Ca^{2+} channel blockers did not alter cell cycle regulation. However, T-channels may be one of several important cellular targets underlying the cytotoxic actions of mibefradil. The lack of apparent effect of T-channel block in the cytotoxic actions of pimozide may reflect a number of factors, including contributions from different cytotoxic pathways, the dose-range over which these individual pathways are activated, and well as time- and voltage-dependent differences in the potency of specific T-channel subtype block with prolonged drug exposure (Arnoult and Florman, 1998; Rossier et al., 1998; Perchenet et al., 2000). Taken together, these results suggest that the Ca^{2+} channel antagonists exert cytotoxic effects via complex interactions that extend beyond their ion channel-blocking activities.

References

Adams JM and Cory S (2001) Life-or-death decisions by the Bcl-2 protein family. *Trends Biochem Sci* **26:**61–66.

Albini A, Noonan DM, Melchiori A, Fassina GF, Percario M, Gentleman S, Toffenetti J, and Chader GJ (1992) Laminin-induced retinoblastoma cell differentiation: possible involvement of a 100-kDa cell-surface laminin-binding protein. *Proc Natl Acad Sci USA* **89:**2257–2261.

Arnoult CVM and Florman HM (1998) Pharmacological properties of the T-type Ca^{2+} current of mouse spermatogenic cells. *Mol Pharmacol* **53:**1104–1111.

Barnes S and Haynes LW (1992) Low-voltage-activated calcium channels in human retinoblastoma cells. *Brain Res* **598:**19–22.

Bernink JLM, Prager G, Schelling A, and Kobrin I (1996) Antihypertensive properties of the novel calcium antagonist mibefradil (Ro 40-5967): a new generation of calcium antagonists. *Hypertension* **27:**426–432.

Bijlenga P, Liu JH, Espinos E, Haenggeli CA, Fischer-Lougheed J, Bader CR, and Bernheim L (2000) T-type alpha 1H Ca^{2+} channels are involved in Ca^{2+} signaling during terminal differentiation (fusion) of human myoblasts. *Proc Natl Acad Sci USA* **97:**7627–7632.

Boyden PA and Jeck CD (1995) Ion channel function in disease. *Cardiovasc Res* **29:**312–318.

Brent PJ, Pang G, Little G, Dosen PJ, and Van Helden DF (1996) The sigma receptor ligand, reduced haloperidol, induces apoptosis and increases intracellular-free calcium levels $[Ca^{2+}]^i$ in colon and mammary adenocarcinoma cells. *Biochem Biophys Res Commun* **219:**219–226.

Chemin J, Monteil A, Briquaire C, Richard S, Perez-Reyes E, Nargeot J, and Lory P (2000) Overexpression of T-type calcium channels in HEK-293 cells increases intracellular calcium without affecting cellular proliferation. *FEBS Lett* **478:**166–172.

Clozel J-P, Veniant M, and Osterrieder W (1990) The structurally novel Ca^{2+} channel blocker Ro 40-5967, which binds to the [^{3}H] desmethoyverapamil receptor, is devoid of the negative ionotropic effects of verapamil in normal and failing rat hearts. *Cardiovasc Drugs Ther* **4:**731–736.

Crawford KW and Bowen WD (2002) Sigma-2 receptor agonists activate a novel apoptotic pathway and potentiate antineoplastic drugs in breast tumor cell lines. *Cancer Res* **62:**313–322.

Enyeart JJ, Biagi BA, Day RN, Sheu SS, and Maurer RA (1990) Blockade of low and

high threshold Ca^{2+} channels by diphenylbutylpiperidine antipsychotics linked to inhibition of prolactin gene expression. *J Biol Chem* **265:**16373–16379.
Enyeart JJ, Mlinar B, and Enyeart JA (1993) T-type Ca^{2+} channels are required for adrenocorticotropin-stimulated cortisol production by bovine adrenal zona fasciculata cells. *Mol Endocrinol* **7:**1031–1040.
Galizzi JP, Fosset M, Romey G, Laduron P, and Lazdunski M (1986) Neuroleptics of the diphenylbutylpiperidine series are potent calcium channel inhibitors. *Proc Natl Acad Sci USA* **83:**7513–7517.
Giuliano M, Lauricella M, Vassallo E, Carabillo M, Vento R, and Tesoriere G (1998) Induction of apoptosis in human retinoblastoma cells by topoisomerase inhibitors. *Invest Ophthalmol Vis Sci* **39:**1300–1311.
Glasser S (1998) The relevance of T-type calcium antagonists: a profile of mibefradil. *J Clin Pharmacol* **38:**659–669.
Gomora JC and Enyeart JJ (1999) Dual pharmacological properties of a cyclic AMP-sensitive potassium channel. *J Pharmacol Exp Ther* **290:**266–275.
Guttridge DC, Albanese C, Reuther JY, Pestell RG, and Baldwin AS Jr (1999) NF-kappaB controls cell growth and differentiation through transcriptional regulation of cyclin D1. *Mol Cell Biol* **19:**5785–5799.
Hirooka K, Bertolesi GE, Kelly MEM, Denovan-Wright EM, Sun X, Hamid J, Zamponi GW, Juhasz AE, Haynes LW, and Barnes S (2002) Expression of T-type calcium channel α1G and α1H in human retinoblastoma cells and their loss after differentiation. *J Neurophysiol*, in press.
Hirooka K, Kelly MEM, Baldridge WH, and Barnes S (2000) Suppressive actions of betaxolol on ionic currents in retinal ganglion cells may explain its neuroprotective effects. *Exp Eye Res* **70:**611–621.
Jänicke RU, Sprengart ML, Wati MR, and Porter AG (1998) Caspase-3 is required for DNA fragmentation and morphological changes associated with apoptosis. *J Biol Chem* **273:**9357–9360.
Kuga T, Kobayashi S, Hirakawa Y, Kanaide H, and Takeshita A (1996) Cell cycle-dependent expression of L- and T-type Ca^{2+} currents in rat aortic smooth muscle cells in primary culture. *Circ Res* **79:**14–19.
Kyritsis AP, Tsokos M, Triche TJ, and Chader GJ (1984) Retinoblastoma—origin from a primitive neuroectodermal cell? *Nature (Lond)* **307:**471–473.
Lacinová L, Klugbauer N, and Hofmann F (2000) Regulation of the calcium channel alpha(1G) subunit by divalent cations and organic blockers. *Neuropharmacology* **39:**1254–1266.
Lee GL and Hait WN (1985) Inhibition of growth of C6 astrocytoma cells by inhibitors of calmodulin. *Life Sci* **36:**347–354.
Lijnen P, Fagard R, and Petrov V (1999) Mibefradil-induced inhibition of proliferation of human peripheral blood mononuclear cells. *J Cardiovasc Pharmacol* **33:**595–604.
Maas RA, Bruning PF, Top B, Breedijk AJ, and Peterse HL (1995) Growth arrest associated changes of mRNA levels in breast cancer cells measured by semi-quantitative RT-PCR: potential early indicators of treatment response. *Cancer Lett* **97:**107–116.
Mishra SK and Hermsmeyer K (1994) Selective inhibition of T-type Ca^{2+} channels by Ro 40-5967. *Circ Res* **75:**144–148.
Mullins ME, Horowitz BZ, Linden DH, Smith GW, Norton RL, and Stump J (1998) Life-threatening interaction of mibefradil and beta-blockers with dihydropyridine calcium channel blockers. *JAMA (J Am Med Assoc)* **280:**157–158.
Nilius B, Prenen J, Kamouchi M, Viana F, Voets T, and Droogmans G (1997) Inhibition by mibefradil, a novel calcium channel antagonist, of Ca^{2+}- and volume-activated Cl^- channels in macrovascular endothelial cells. *Br J Pharmacol* **121:**547–555.
Perchenet L, Benardeau A, and Ertel EA (2000) Pharmacological properties of Ca(V)3.2, a low voltage-activated Ca^{2+} channel cloned from human heart. *Naunyn Schmiedeberg's Arch Pharmacol* **361:**590–599.
Rossier MF, Ertel EA, Vallotton MB, and Capponi AM (1998) Inhibitory action of mibefradil on calcium signaling and aldosterone synthesis in bovine adrenal glomerulosa cells. *J Pharmacol Exp Ther* **287:**824–831.
Rouzaire-Dubois B and Dubois JM (1998) K^+ channel block-induced mammalian neuroblastoma cell swelling: a possible mechanism to influence proliferation. *J Physiol* **510:**93–102.
Rutledge A and Triggle DJ (1995) The binding interactions of Ro 40-5967 at the L-type Ca^{2+} channel in cardiac tissue. *Eur J Pharmacol* **280:**155–158.
Schmitt R, Clozel JP, Iberg N, and Buhler FR (1995) Mibefradil prevents neointima formation after vascular injury in rats. Possible role of the blockade of the T-type voltage-operated calcium channel. *Arterioscler Thromb Vasc Biol* **15:**1161–1165.
Sola B, Salaun V, Ballet JJ, and Troussard X (1999) Transcriptional and post-transcriptional mechanisms induce cyclin-D1 over-expression in B-chronic lymphoproliferative disorders. *Int J Cancer* **83:**230–234.
Strobl JS, Kirkwood KL, Lantz TK, Lewine MA, Peterson VA, and Worley JF (1990) Inhibition of human breast cancer cell proliferation in tissue culture by the neuroleptic agents pimozide and thioridazine. *Cancer Res* **50:**5399–5405.
Strobl JS, Melkoumian Z, Peterson VA, and Hylton H (1998) The cell death response to gamma-radiation in MCF-7 cells is enhanced by a neuroleptic drug, pimozide. *Breast Cancer Res Treat* **51:**83–95.
Vilner BJ and Bowen WD (2000) Modulation of cellular calcium by sigma-2 receptors: release from intracellular stores in human SK-N-SH neuroblastoma cells. *J Pharmacol Exp Ther* **292:**900–911.
Vilner BJ, John CS, and Bowen WD (1995) Sigma-1 and sigma-2 receptors are expressed in a wide variety of human and rodent tumor cell lines. *Cancer Res* **55:**408–413.
Wang TT and Phang JM (1995) Effects of estrogen on apoptotic pathways in human breast cancer cell line MCF-7. *Cancer Res* **55:**2487–2489.
Wondergem R, Gong W, Monen SH, Dooley SN, Gonce JL, Conner TD, Houser M, Ecay TW, and Ferslew KE (2001) Blocking swelling-activated chloride current inhibits mouse liver cell proliferation. *J Physiol* **532:**661–672.

Address correspondence to: Melanie E. M. Kelly, Ph.D., Department of Pharmacology, Dalhousie University, Halifax, Nova Scotia, B3S 4H7 Canada. E-mail: mkelly@is.dal.ca